行政院國家科學委員會補助專題研究計畫成果報告

※※※※※※※※※※※※※※※※※※※※※※※※※※※※※※※※
※ ※
※ **新型光電材料、元件及雷射光源(II) –** ※
※ **子計畫一：新型半導體、光纖及非線性光學元件** ※
※ ※
※※※※※※※※※※※※※※※※※※※※※※※※※※※※※※※※

計畫類別：☐ 個別計畫　■ 整合型計畫

計畫編號：**NSC 89-2215-E-002-035**

執行期間：**88 年 8 月 1 日 至 89 年 10 月 31 日**

計畫主持人：楊　志　忠

本成果報告包括以下應繳交之附件：

☐ 赴國外出差或研習心得報告一份
☐ 赴大陸地區出差或研習心得報告一份
■ 出席國際學術會議心得報告及發表之論文各一份
☐ 國際合作研究計畫國外研究報告書一份

執行單位：　國立台灣大學光電所

中　華　民　國　九十　年　一　月　二　日

國科會專題研究結案報告

新型光電材料、元件及雷射光源(II) –
子計畫一：新型半導體、光纖及非線性光學元件
Novel Semiconductor, Fiber, and Nonlinear Optics Devices

計畫主持人： 楊志忠　　執行單位： 國立台灣大學光電所

計畫編號： NSC 89-2215-E-002-035
執行期限：88 年 8 月 1 日至 89 年 10 月 31 日

中文摘要：

光纖方面，我們已製作超音波調制光纖布拉格光柵來從事布拉格反射率之調變、反射波長之調變及 Q-開關掺鉺光纖雷射。半導體元件方面，我們已觀察到在一外腔半導體雷射鎖模機制之自調變。至於非線性光學元件方面，我們提出利用光柵來對不完整週期之週期反轉鈮酸鋰晶體做相位補償之觀念，同時，我們也和合作夥伴製作以鈦寶石雷射來泵激 KTP 晶體之光參數振盪器。

Abatract:

We have implemented acoustically modulated fiber Bragg grating devices for Bragg reflection modulation, reflection wavelength switching, and Q-switched erbium-doped fiber laser. On semiconductor devices, we have observed self-modulation of mode-locking mechanism in an external-cavity semiconductor laser. Regarding nonlinear-optics devices, we have proposed the use of a grating structure for phase-compensation in a PPLN crystal of incomplete period. Also, with collaborators we have implemented optical parametric oscillators with KTP crystals, pumped with Ti:sapphire lasers.

I. Fiber Devices:

1) We report a novel device of modulating the Bragg reflectivity of a fiber grating by exciting the transverse vibration of the fiber through an acoustic wave. The excitation of the transverse vibration, leading to fiber micro bending, induces the coupling of the fiber core mode into cladding modes. This leads to the reduction of core-mode power and hence that of Bragg reflection. This mechanism provides us a means to control the reflectivity after a fiber Bragg grating is fabricated. The numerical results based on a simple micro-bending model agree well in trend with the experimental data.
2) Coupling between co-propagating core modes and cladding modes was implemented by acoustically generating lateral vibration of an etched fiber. When these coupling processes were combined with counter-propagating coupling of a core mode and a cladding mode and the Bragg reflection of a fiber grating, switching of reflection wavelength between the Bragg wavelength and cladding-mode coupling wavelengths was achieved. We report the implementation of such acoustically induced switching behaviors and explain their operation principles. The implemented results can be used for WDM add/drop filtering.
3) An actively Q-switched all-fiber laser based on an acoustically modulated fiber attenuator was implemented for producing 1550.5 nm pulses of 3 μJ in pulse energy, 150 nsec in pulse width, and 5 kHz in pulse repetition frequency. The fiber attenuator was combined with a fiber Bragg grating, which was used as the end mirror and the wavelength selector of the laser system. The fiber attenuator was implemented with the excitation of transverse vibration by a modulated acoustic wave. The transverse vibration or micro bending led to the coupling of the core mode and cladding modes. Through this mechanism, the

feedback level from the fiber grating or the Q factor of the laser can be well controlled. The Q-switched fiber laser based on this scheme can be quite simple.

II. Semiconductor Devices

1) We report the observed results of self modulation of passive mode-locking mechanism in an external-cavity semiconductor laser, in which a slant ridge-loading waveguide was formed for the gain medium. A region beside the ridge at a cleaved end of the waveguide served as a saturable absorber for mode-locking and its modulation. Under different conditions of injection current and cavity alignment, we observed three laser operation regimes, including pure cw oscillation, constant mode-locked and cw components coexistent, and modulated mode-locked and cw components coexistent. The mode-locking modulation phenomenon is different from the previously reported concurrence of mode-locking and self-pulsation. A model was proposed to explain well the observed results.

III. Nonlinear-optics Devices

1) An incomplete period of the last quasi-phase-matching (QPM) segment in a periodically poled nonlinear crystal represents a key problem in implementing a nonlinear wavelength conversion device with round-trip or oscillating waves of interaction. Such a segment at the crystal end implies the broken QPM periodicity for the reflected waves of interaction. Here, we demonstrate numerically that with a grating structure at the crystal end for reflecting signal, the wavelength-dependent phase shift at Bragg reflection can compensate the phase mismatch of the reflected signal, idler and pump of an optical parametric process. Therefore, by slightly shifting the signal wavelength the phase-matching condition can be maintained with any length of the last QPM segment. It was shown that with the grating structure, the conversion efficiency of the round-trip optical parametric process could always be optimized.
2) We report the implementation of a KTP optical parametric oscillator pumped by a pulsed Ti:sapphire laser. Including signal and idler, it could be continuously tuned from 1.261 through 2.532 μm by varying the pump wavelength. Two major improvements were achieved, including the connection of the signal and idler tuning ranges and the high output pulse energy through the signal and idler tuning ranges. The first improvement was achieved by discovering two particular sets of phase-matching angles. The second improvement was realized by using five sets of resonator mirrors for oscillating either signal or idler. Theoretical calculations were also conducted for the effective nonlinear coefficient, walk-off angle, phase-matching acceptance angle, and output spectral widths for the concerned phase-matching angles. The second part of this paper presents the experimental and theoretical results of sum-frequency mixing of a Ti:sapphire laser and a 1.064 μm Nd:YAG laser. By using two KTP crystals cut at $\theta = 76$ and 85° ($\phi = 90^{\circ}$ in both crystals), respectively, we have experimentally achieved sum-frequency mixing tuning range from 459.3 through 472.9 nm. The energy conversion efficiencies were reasonably high.

Related Journal Publication List:

1. Chih-Wei Hsu and C. C. Yang, "Using a Grating Structure for Phase Compensation in Achieving Efficient Round-trip Optical Parametric Process in PPLN with an Incomplete QPM Period," Optics Letters, Vol. 24, pp. 540-542, 1999.
2. D. W. Huang, W. F. Liu, C. W. Wu and C. C. Yang, "Reflectivity-tunable Fiber Bragg Grating Reflectors," IEEE Photonics Technology Letters, Vol. 12, pp. 176-178, 2000.
3. Chih-Chang Chen, Yean-Woei Kiang and

C. C. Yang, "Colliding-pulse Mode-locked Semiconductor Laser with a Multimode-interference Waveguide Amplifier," Optics Communications, Vol. 177, pp. 363-368, 2000.

4. Yih-Jun Wong, Hong-Hsieng Chen, Choong-Wen Lai, Yean-Woei Kiang, and C. C. Yang, "Self-modulation in an External-cavity Semiconductor Laser," Optics Communications, Vol. 180, pp. 317-321, 2000.
5. Wen-Fung Liu, I-Ming Liu, Lung-Wei Chung, Ding-Wei Huang, and C. C. Yang, "Acoustics-Induced Reflection Wavelength Switching in a Fiber Bragg Grating," Optics Letters, Vol. 25, no. 18, pp. 1319-1321, 2000.
6. D. W. Huang, W. F. Liu, and C. C. Yang, "Q-Switched Fiber Laser with an Acoustically Modulated Fiber Attenuator," IEEE Photonics Technology Letters, Vol. 12, no.9, pp. 1153-1155, 2000.
7. Cheng-Yen Chen, Kung-Jeng Ma, Yen-Shen Lin, Chung-Yen Chao, Steffen Gurtler, Chee-Wee Liu, Chih-Wei Hsu, and C. C. Yang, "Formation of Silicon Surface Gratings with High Pulse-Energy UV Laser," J. Applied Physics, December, 2000.
8. J. Q. Yao, X. Ding, J. Y. Qiao, C. C. Yang, I. J. Hsu, and C. W. Hsu, "Pump-Tuning Optical Parametric Oscillation and Sum-Frequency Mixing with KTP Pumped by a Ti:sapphire Laser," accepted for publication in Optics Communication.
9. Yan-Ju Chiang, Likarn Wang, Wen-Fung Liu, Horng-Shyang Chen, Chih-Wei Hsu, and C. C. Yang, "Temperature-Insensitive Strain Measurement Using Two Fiber Bragg Gratings in a Power Detection Scheme," submitted to IEEE Photonics Technology Letters.

出國參加會議報告

一、參加 1999 年 Conference on Lasers and Electro-Optics / Pacific Rim（CLEO PR）

1. 時間：88 年 9 月 28 日-10 月 2 日
2. 地點：韓國漢城
3. 開會經過：除了發表三篇文章並參與五天會議外，最重要的，本人代表我國參加 CLEO/PR 的 Steering Committee 會議，爭取 2003 年 CLEO/PR 在台北的舉辦權。我們競爭對手為澳洲雪梨。當時開會時，場面相當熱烈，會議結束時，我國與澳洲的勝算平分秋色。
4. 與會心得：欲在國際上競爭，自己得有些實力才行。兩岸的對立情況，使得我國在國際上活動不太順暢。

二、參加 2000 年 Optical Fiber Communication Conference（OFC）

1. 時間：89 年 3 月 6 日-3 月 11 日
2. 地點：美國巴爾的摩
3. 開會經過：這次開會有兩件事情值得一提，一為感受到美國或全球光通訊的熱潮，由於網路的需求，光纖通訊成為熱門行業，本次會議參加人數也暴增為兩倍，為主辦單位美國光學學會預料未及。另一件事值得一記的是，本人代表我國爭取 CLEO/PR2003 主辦權於 Steering Committee 開會時，經多方爭取，終於成功。
4. 與會心得：看看美國與我國光纖通訊產業界的熱潮，倒顯得我們政府決策相關人士之動作太慢，實在趕不上時代的需求。

Formation Mechanism Dependence on Laser Power of UV-laser Ablated Silicon Surface Gratings

Cheng-Yen Chen, Steffen Gurtler, C. C. Yang
Institute of Electro-Optical Engineering, National Taiwan University,
1, Roosevelt Road, Sec. 4, Taipei, Taiwan, R.O.C.
(Tel) 886-2-23657624 (Fax) 886-2-23652637 (E-mail) ccy@cc.ee.ntu.edu.tw
Kung-Jeng Ma
Department of Mechanical Engineering, Chung Cheng Institute of Technology,
Ta-Shi, Taoyuan, Taiwan, R.O.C.

Silicon surface gratings are useful for temperature control in IC process and optoelectronics applications. They can be easily fabricated with laser ablation. In this paper, we report our results of UV-laser ablated silicon surface gratings. It was found that different laser-matter interactions were involved for forming the surface gratings when different levels of laser power were used. Hence, different morphologies of gratings were observed. In fabricating a grating, a silicon wafer was exposed to the interference fringes formed through a prism or a holographic system with the fourth-harmonic (266 nm) of a Q-switched Nd:YAG laser. With the prism method, the grating period can be varied from 180 through 600 nm. Figure 1 shows the atomic force microscopic (AFM) picture of a silicon surface grating with the period at 400 nm. The grating was formed with 14 mJ/cm^2 laser fluence with 30 Hz pulse repetition rate for 15 sec (i.e., 450 pulse shots) in the atmosphere. It was identified that the formation of the corrugations was due to silicon oxidation process. The crests shown in the figure are silicon oxide. From the Fourier transform infrared spectroscopy study, the oxide is oxygen deficient, i.e., SiO_x ($x < 2$). Also, it was discovered that the oxidation process would be more efficient with ambient water vapor, compared with ambient oxygen molecules. The existence of oxide was proved with energy dispersive X-ray spectroscopy and HF etching. Figure 2 shows the AFM picture of the grating of Fig. 1 after HF dipping. After silicon oxide was removed, the crests became valleys. Figure 3 shows the real-time monitoring of the first-order diffracted signal intensity variation with number of laser shots. The results were obtained using the holographic system We can see that the diffraction becomes detectable after 700 shots in this situation. The slightly irregular variation of the diffracted intensity was attributed to mechanical instability. To see the dependence on laser power level, we increased the laser fluence to 60 mJ/cm^2. Figure 4 shows the diffracted intensity variation with the number of laser shots. The spiky features shown here are similar with ambient water vapor and ambient nitrogen, indicating that the rapid formation and destruction have nothing to do with silicon oxidation. It is believed that this process is due to quick melting and sputtering. Again, the destruction of grating is caused by mechanical instability. To further understand this ablation process, we exposed the sample with only one laser shot at 60 mJ/cm^2. Because of aberration in our laser interference system, a fringe of a larger period was formed besides the designated interference fringe. Figures 5 and 6 show the AFM pictures of the grating at a high and a low intensity beam portions, respectively. From Fig. 5, we can see that at the highest intensity sharp peaks with valleys on both sides were formed. Then, at the medium intensity double peaks with three valleys were produced. At the lowest intensity, nothing is visible. Note that after HF dipping, the structures in Figs. 5 and 6 still existed, indicating that their formation was not due to silicon oxidation. More detailed results, including the data of energy dispersive X-ray spectroscopy and the origins of the different surface morphologies, will be discussed.

0-7803-5661-6 / 99 / $10.00

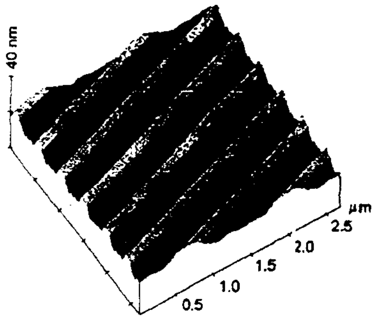

Fig. 1 AFM picture of an oxide grating.

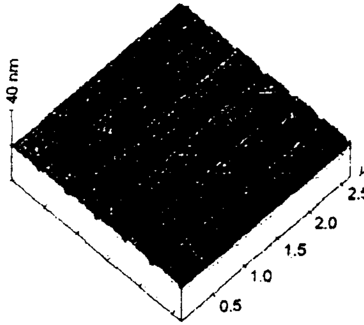

Fig. 2 AFM picture after HF dipping.

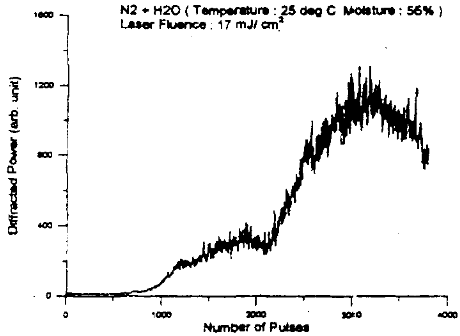

Fig. 3 Growth of an oxide grating.

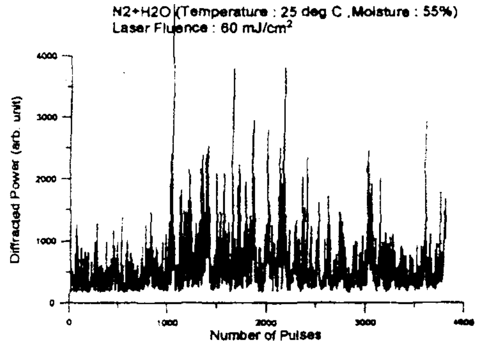

Fig. 4 Evolution of an ablated grating.

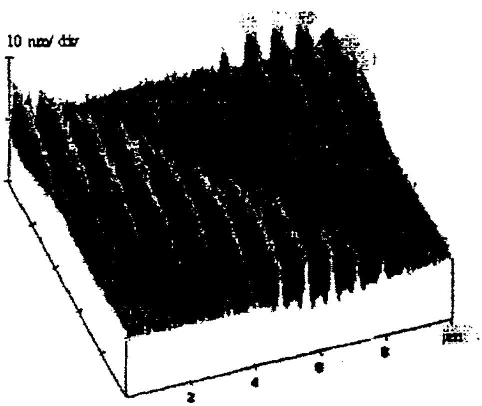

Fig.5 AFM picture after single-shot exposure.

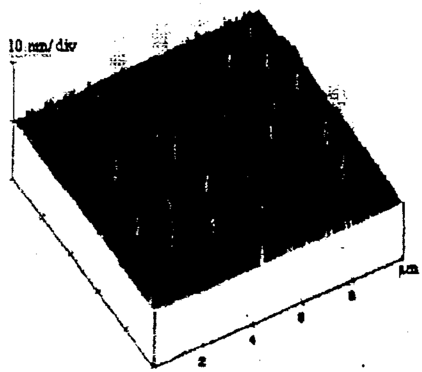

Fig. 6 AFM picture of another portion.

Pump-Probe Study on Nonlinear Switching in an All-Active-Semiconductor-Optical-Amplifier Loop Device

Jiun-Haw Lee, Ding-An Wang, Hsin-Jiun Chiang, Ding-Wei Huang, Steffen Gurtler, Yean-Woei Kiang, and C. C. Yang

Department of Electrical Engineering and Institute of Electro-Optical Engineering, National Taiwan University, 1, Roosevelt Road, Sec. 4, Taipei, Taiwan, R.O.C.

Tel: 886-2-23657624 Fax: 886-2-23652637 E-mail: ccy@cc.ee.ntu.edu.tw

We report the pump-probe study results of the nonlinear switching behaviors in an all-active-semiconductor-optical-amplifier loop device as depicted in Fig. 1. The ridge-loading waveguide loop has a radius 300 μm with a ridge width 4 μm. The loop is connected to a multi-mode interference (MMI) waveguide with a length 500 μm and a ridge width 8 μm which serves as the nonlinear element. Then, the input and output ports are also 4 μm waveguides with both lengths about 100 μm. For injecting different currents in different areas, we divided the electro-pad into four disconnected regions, indicated by the injection currents I_1 (input/output region), I_2 (MMI region), I_3 (one-quarter of loop) and I_4 (three-quarter of loop). Figure 2 demonstrates three sets of data showing power-dependent switching. We launched a cw Ti:sapphire laser at 849.6 nm, which corresponded to the gain peak of the TE polarization, with various power levels and monitored the output power variation at the same wavelength. The horizontal axis in Fig. 2 shows the input power before entering the input waveguide. In this measurement, I_1 = 30 mA, $I_3 + I_4$ = 300 mA and the I_2 value is shown in the figure. Because the guiding layer of the amplifier waveguide was so thin (only about 0.3 μm), the input coupling efficiency was estimated to be only on the order of 0.1 % or even smaller. All three curves show depression of output power when the input power reaches certain values. The observed nonlinear switching behavior comes from the effect of the nonlinear coupling in the MMI waveguide region. This mechanism is different from that in a typical Sagnac interferometer which the nonlinear optical mechanism comes from the loop. The loop has the function of providing gain to the optical signals and redistributing the lateral wave field. Although the nonlinear optical mechanism comes from the MMI amplifier, the loop still plays a crucially important function. Figure 3 illustrates the simulation results for the four cases: loop with gain (normal function of the device), loop without gain (a small $I_3 + I_4$ for the device), mirror with gain (loop removed with an assumed gain), and mirror without gain (loop removed). We can see that only in the case of "loop with gain", efficient nonlinear switching can be observed.

Figures 4 shows the experimental setup for the cw pump-probe measurement. The two independent tunable Ti:Sapphire lasers were used to study the cross effect of two input signals of different wavelengths/polarization. The output signals passed a monochromator which was used as a spectral filter to eliminate the unwanted amplified spontaneous emission. In Fig. 5 (6), we demonstrate several sets of data with input power of the signal at 847.2 nm (849.6 nm) varied from 0 to 15 mW. The horizontal axis represents the input power at 849.6 nm (847.2 nm) and the vertical axis stands for the output power at the same wavelength. As shown in Fig. 5, the output power at 849.6 nm is affected by the input signal at 847.2 nm although the gain at 849.6 nm is higher. When the input power at 847.2 nm reaches 10 mW, the nonlinear switching effect becomes insignificant. On the other hand, from Fig. 6 the output power at 847.2 nm is not strongly affected by the input power at 849.6 nm.

In summary, we have fabricated all-semiconductor-optical-amplifier loop devices and characterized their operation with cw signals. Gain saturation in the MMI coupler led to nonlinear coupling and hence the power-dependent switching of the devices. The active loop is important to provide gain and to redistribute the field.

0-7803-5661-6 / 99 / $10.00

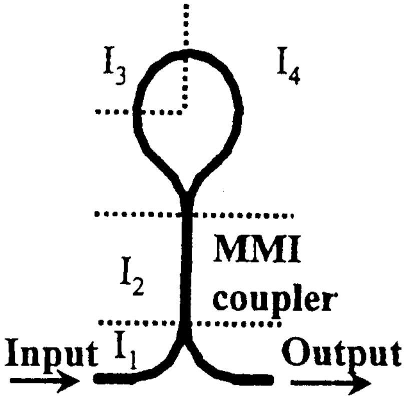

Fig.1 Layout of the device.

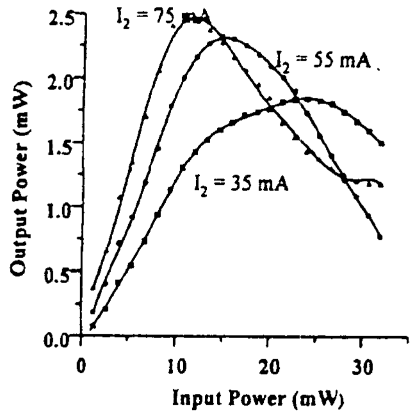

Fig.2 Output power as a function of input power with different I_2 values.

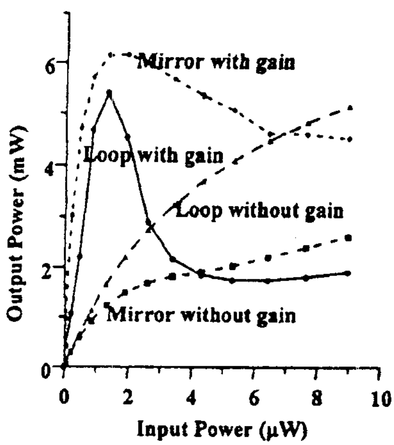

Fig.3 Simulation results with different device stuctures.

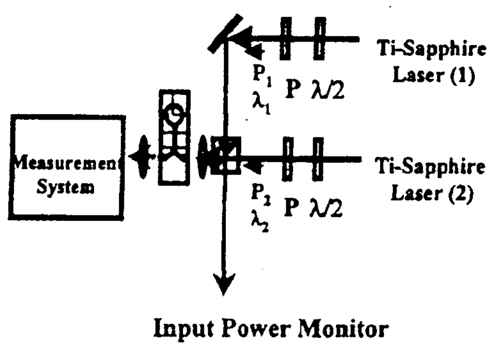

Fig.4 Experiment setup of cw pump-probe system.

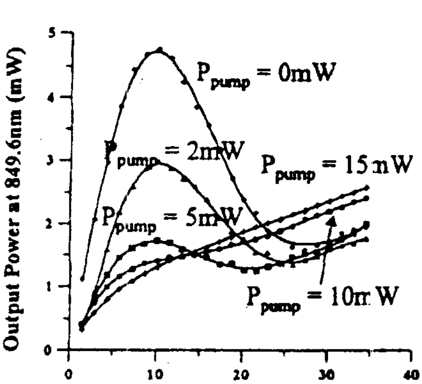

Fig.5 Output power as a function of input probe power (at 849.6 nm) with different input pump power (at 847.2 nm)

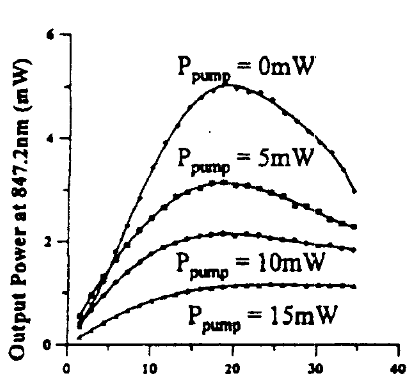

Fig.6 Output power as a function of input probe power (at 847.2 nm) with different input pump power (at 849.6 nm)

Monolithic PPLN-based Optical Parametric Oscillators Using Grating Structures for Phase Compensation in Achieving Efficient Round-trip Wavelength Conversion

Chih-Wei Hsu, Cheng-Yen Chen and C. C. Yang
Institute of Electro-Optical Engineering, National Taiwan University,
1, Roosevelt Road, Sec. 4, Taipei, Taiwan, R.O.C.
(phone) 886-2-23657624 (fax) 886-2-23652637 (E-mail) ccy@cc.ee.ntu.edu.tw

With the development of domain inversion techniques for quasi-phase matched $LiNbO_3$ and other nonlinear optical materials, wavelength conversion efficiencies for frequency doubling and optical parametric processes have been tremendously increased [1]. However, so far all oscillators based on quasi-phase-matching (QPM) materials for wavelength conversion were made with the configuration of external cavity. It is a natural trend to develop compact monolithic wavelength converter. Such a device can be implemented by preparing high-reflection coating on the end-facets of a QPM material to reduce the oscillation threshold. However, such an arrangement faces a basic problem, i.e., the length of the last QPM segment at the material end facet is uncontrollable because the period of QPM ranges from a few μm to a few tens μm. Unless the length of the last QPM period is exactly equal to one-quarter of the QPM period (the optimum situation), the reflected signal from the end-facet will experience broken QPM periodicity and suffer from reduced wavelength conversion efficiency or even reverse energy flow of wavelength conversion [2]. This problem can possibly be solved by preparing anti-reflection coating for one of the pump, signal and idler waves. However, since high-reflection coating needs to be prepared for the other one or two waves at the same time to reduce the oscillation threshold, the coating process becomes quite difficult.

In this paper, we propose the idea of using a grating structure for solving the problem of the incomplete QPM period and demonstrate the simulation results of the phase compensation in achieving efficient round-trip optical parametric oscillation in PPLN. Figure 1 shows the layout of the a monolithic optical parametric oscillator (OPO) with two surface gratings at both ends. The two gratings are chirped to guarantee that their phase variations over the Bragg reflection windows are larger than 2π. One of them has a length of 1 mm and the other has a length of 0.8 mm. The pump input is applied from the long grating side and the signal output is obtained from the short grating side. The whole PPLN length is 5 mm. For our numerical study, we consider the pump wavelength at 1064 nm and signal wavelength at 1550 nm. The idler wavelength is hence at 3.393 μm. The corresponding QPM period of PPLN is 29.6 μm. The central grating period is 361.83 nm, which corresponds to the Bragg wavelength 1550 nm. To obtain numerical results, we solved the coupled equations for the forward and backward pump complex amplitudes, the forward and backward signal complex amplitudes, and the forward and backward idler complex amplitudes.

The symbolic data points in Fig. 2 (3) show the output signal intensity as a function of the signal wavelength within the Bragg reflection window for various L_l values of the grating of 1 (0.8) mm. Here, L_l is the length of the last QPM segment in terms of the QPM period Γ. Before the grating, there is a plain PPLN of 4 (4.2) mm in length. At the crystal end, the signal experiences uncoated end-facet reflection besides the Bragg reflection from the grating. Meanwhile, the idler and the residual pump are reflected from the uncoated and high-reflection (100 %) end-facets, respectively. For comparison, the data curves without symbols in Figs. 2 and 3 show the similar cases without the grating sections. In these cases, the end-facet is high-reflection coated for the signal. The pump intensity is fixed at 500 MW/cm². The initial signal and idler intensities at the left end are set at 0 and 1.25 kW/cm², respectively. We can see that with the grating the output signal intensity oscillates with wavelength. The maximum of the oscillation reaches the level of the optimum situation of the coating device and the minimum has a level about the same as the worst situation of the coating device. The oscillating output signal intensity is attributed to the signal phase variation with wavelength upon reflecting from the grating. At the peaks, the phase of the reflected signal has a value such that the phase-matching condition among the reflected pump, signal and idler is reached for the optimum nonlinear conversion. The results in Fig. 2 imply that with the grating structure, the system will provide the output with the optimum nonlinear conversion by slightly shifting the signal wavelength within the Bragg reflection window of the grating. The wavelength shift is quite small, as small as a few tenths of nm. Such a shift is always within the QPM window

0-7803-5661-6 / 99 / $10.00 © 1999 IEEE

for efficient nonlinear conversion. Because of the difference in grating length between Figs. 2 and 3, the wavelengths for optimum wavelength conversion are different.

Then, we conducted numerical simulations on the whole PPLN with the two gratings. It was observed that the wavelength for optimum OPO signal output resulted from the compromise between the optimum conditions of the two gratings. It also depended on various conditions, such as the input pump power and the length of the central portion of the PPLN resonator. The details of the compromise for the optimum condition and the dependencies on various conditions will be discussed in this paper. Regarding the technique of forming the surface gratings, although chemical wet etching is not a good technique for fabricating corrugation gratings on periodically poled nonlinear crystals because the etching rates of the opposite domains are different, surface gratings on $LiNbO_3$ have been successfully fabricated with laser ablation. Figure 4 shows an atomic force microscopy picture of a surface grating on $LiNbO_3$. The details of this technique will also be discussed.

References:

1. G. D. Miller, R. G. Batchko, W. M. Tulloch, D. R. Weise, M. M. Fejer and R. L. Byer, Opt. Lett. **22**, 1834 (1997).
2. G. Imeshev, M. Proctor and M. M. Fejer, Opt. Lett. **23**, 165 (1998).

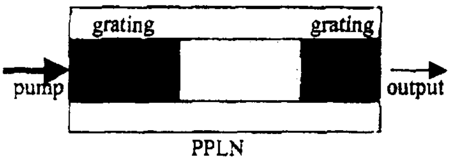

Fig. 1 Layout of the PPLN OPO with surface gratings.

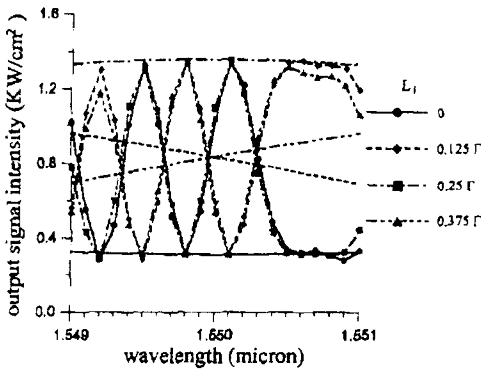

Fig. 2 Output signal intensity versus L_1 of the long grating.

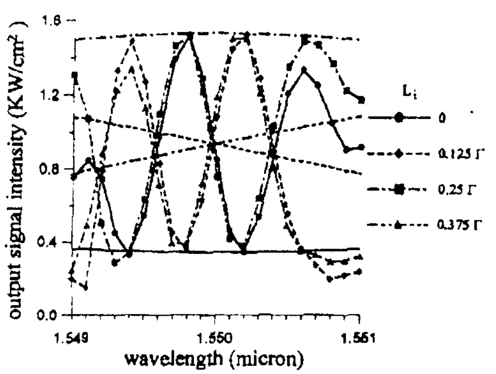

Fig. 3 Output signal intensity versus L_1 of the short grating.

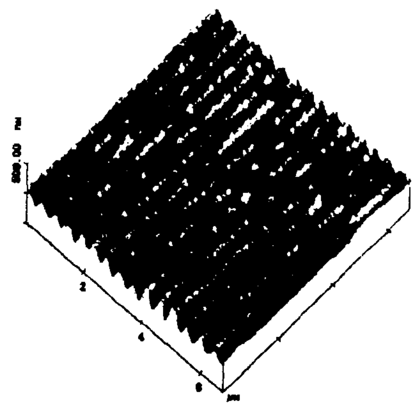

Fig. 4 AFM picture of a $LiNbO_3$ surface grating.

Actively Q-Switched All-Fiber Laser with a Fiber Bragg Grating of Variable Reflectivity

Ding-Wei Huang
Department of Electrical Engineering and Graduate Institute of Electro-Optical Engineering, National Taiwan University, Taipei, Taiwan, R.O.C.
Wen-Fung Liu
Department of Electrical Engineering, Chung Cheng Institute of Technology, Tahsi, Taoyuan, Taiwan, R.O.C.
C. C. Yang
Department of Electrical Engineering and Graduate Institute of Electro-Optical Engineering, National Taiwan University, 1, Roosevelt Road, Sec. 4, Taipei, Taiwan, R.O.C.
phone: 886-2-23657624 fax: 886-2-23652637 E-mail: ccy@cc.ee.ntu.edu.tw

Q-switching of erbium-doped fiber laser can provide simple and robust high-pulse-energy light sources for various applications, including eye-safe ranging, remote sensing, medicine, and others. Typically, external-cavity acousto-optical modulation was used for implementing Q-switching. However, the required external-cavity configuration represents a drawback, which is open for improvement. It is expected that an all-fiber Q-switched laser can increase the efficiency and its robustness. In this paper, we report a novel Q-switched fiber laser based on an acoustically modulated fiber Bragg grating reflector. We used a fiber Bragg grating as the end mirror of the laser cavity. This fiber grating was under acoustic perturbation for controlling its Bragg reflectivity. Therefore, the Q-factor of the laser cavity was switched high and low by the acoustic wave. Pulses of around 150 nsec in width and 7.6 μJ in pulse energy were obtained. The laser slope efficiency was 13.1 %. This all-fiber Q-switched fiber laser can be quite compact and robust.

Figure 1 shows the experimental setup of the Q-switched fiber laser. Right to the 72-cm long erbium-doped fiber, it was spliced to a fiber Bragg grating with the Bragg wavelength at 1550.5 nm. Between the grating and erbium-doped fiber, the fiber was laterally glued onto the tip of a metal horn (made of aluminum), whose base was attached to a piezoelectric transducer (PZT), driven by a voltage source, for receiving mechanical vibration. This is the part of the setup for producing acoustic perturbation of the fiber grating. Left to the erbium-doped fiber, a WDM fiber coupler was connected for providing 980 nm pump power, which was provided by an argon-laser pumped Ti:sapphire laser. To the very left end, the cleaved fiber facet was used as the output coupler of the laser and provided about 4 % reflectivity. The whole cavity length was 136 cm.

The fiber grating has a length of 1.5 cm and a Bragg reflection window of 0.5 nm, centered at 1550.5 nm. The peak reflectivity was about 95 %. To concentrate the incoming acoustic power near the core of the fiber, the cladding of the fiber grating section was etched with HF solution to reduce the cladding diameter down to 30 μm. The length of this minimum cladding diameter was 2 cm with the 1.5-cm long grating located at the center. Including the two taper sections on both sides, the whole etched fiber length was about 5 cm. The metal horn was 1 cm in base diameter and 1.5 cm in length. Its tip was glued to the fiber about 2.5 cm from the grating center. Its base was glued to a thin PZT of 1.3 cm in diameter and 1.8 mm in thickness. The PZT was connected to a voltage source for driving acoustic waves. The acoustic waves propagated with increasing intensity along the horn to its tip and translated the power to the fiber. With the acoustic excitation, the fiber vibrated transversely to create micro-bending. The micro-bending produced the optical coupling between the core mode and cladding modes of the fiber. The cladding-mode power decayed through radiation. The out-coupling of optical core-mode signal reduced the power for Bragg reflection of the grating. Therefore, Bragg reflectivity of the fiber grating decreased with the intensity of the acoustic wave or the applied voltage to the PZT. Figure 2 shows the variation of Bragg reflection spectrum with various applied voltage levels when the acoustic frequency is 713 kHz. One can see that as the peak-to peak (p-p) voltage increases to 68.8 V, the Bragg reflectivity near 1550.5 nm is reduced to almost zero. This is the acoustic perturbation mechanism for Q-switching.

To see the response speed of the acoustic control of Bragg reflectivity, we applied a periodical square-wave modulation with various frequencies to the sinusoidal voltage signal at 713 kHz. Figure 3 shows the modulation response when the modulation frequency is 5 kHz. Part (b) of this figure shows the applied sinusoidal voltage under 5 kHz modulation with 50 % duty cycle. Part (a) shows the variation of Bragg reflectivity at 1550.5 nm of the fiber grating. One can see that switch-off of Bragg reflectivity is faster than switch-on as the acoustic wave is turned on and then off. The switching time depends on several parameters, including sound speed in fiber, the location of the horn tip along the fiber, the length of fiber grating, and the masses of the metal horn and PZT. The reflectivity starts to recover about 40 μsec after the voltage is turned off. Before turn-on of acoustic wave of the next cycle, only 60 μsec left for reflectivity recovery. Because of the slow recovery and fast decay of Bragg reflectivity, the reflectivity value fluctuates between 0.06 and 0.27. Note that because the sampling rate of the used oscilloscope was not well set, the fast oscillation of the applied voltage in Fig. 3 does not represent the real acoustic frequency.

Figure 4 shows the laser output pulse profile and the applied voltage. Here, the Q-switching frequency was 5 kHz, the applied voltage was 72 V (p-p), and the acoustic frequency was 713 kHz. The 980 nm pump power was 290 mW. This figure shows that the pulse width is about 150 nsec. The laser threshold is near 2 mW and the slope efficiency is about 13.1 %. Take the case of 290 mW pump power as an example, it corresponds to the average output power of 38 mW or pulse energy of 7.6 µJ/pulse. With the pulse width of 150 nsec, the peak power is 50.7 W. It is believed that the pulse energy can be scaled up for at least several times.

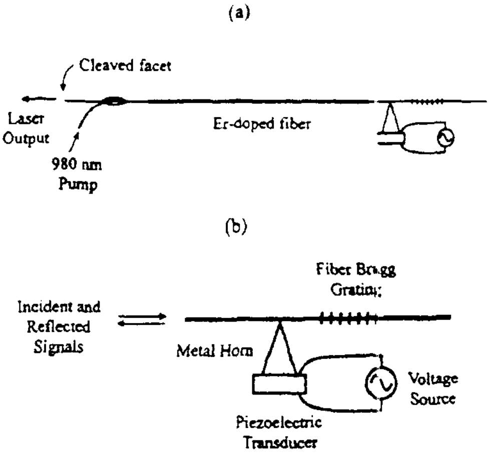

Fig. 1 Experimental setup of the Q-switched laser.

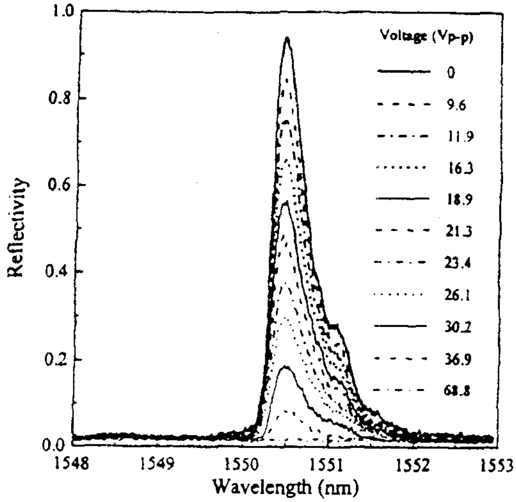

Fig. 2 Bragg reflection spectrum variation with various applied voltage levels.

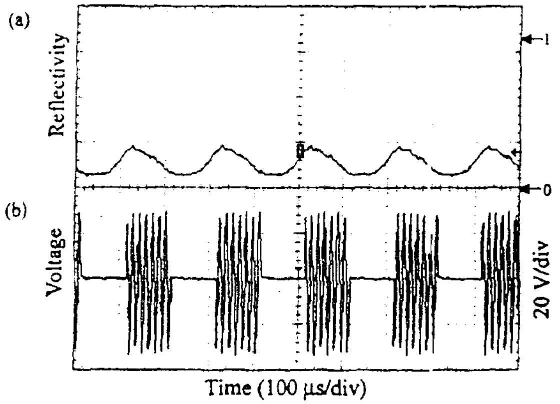

Fig. 3 (a) Bragg reflectivity response to a square-wave modulation of acoustic wave with modulation frequency at 5 kHz; (b) Variation of the applied voltage.

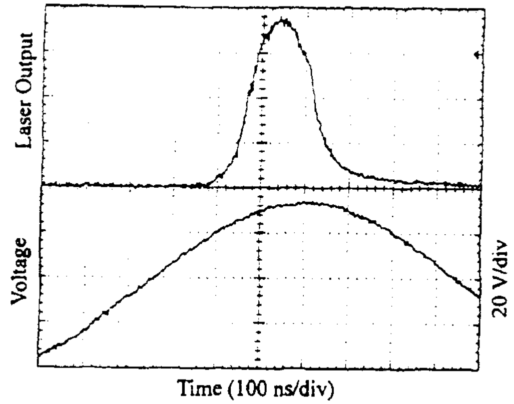

Fig. 4 Laser output pulse shape and the modulated applied voltage.